Journal of the Brazilian Society of Mechanical Sciences and Engineering (2020) 42:475
https://doi.org/10.1007/s40430-020-02553-6

TECHNICAL PAPER

# Estimating Lyapunov spectrum on shape-memory alloy oscillators considering cloned dynamics and tangent map methods

Daniel M. Barreto Netto[1,2] · Alex Brandão[2] · Alberto Paiva[3] · Pedro M. C. L. Pacheco[1] · Marcelo A. Savi[2]

Received: 10 January 2020 / Accepted: 4 August 2020 / Published online: 17 August 2020
© The Brazilian Society of Mechanical Sciences and Engineering 2020

**Abstract**
Mechanical devices built with shape-memory alloys become popular due to thermomechanical coupling associated with solid-state phase transformations. The main characteristics stemming from these transformations are the intrinsic dissipation and the change of thermomechanical properties as a consequence of the phase transformations. Shape-memory alloy oscillators have a nonlinear behavior that can reach responses with different natures such as periodic, quasiperiodic, chaotic, or even hyperchaotic. A proper identification of these behaviors requires the use of dynamical tools, and among them, Lyapunov exponents are one of the most relevant. This work deals with the calculation of the Lyapunov spectrum of shape-memory alloy oscillators. One- and two-degree-of-freedom systems are of concern. Two different approaches are compared: the classical algorithm that uses a tangent space approach; and the cloned dynamics algorithm that is a Jacobian-free approach. Results show that both methods have similar results, allowing the use of cloned dynamics as an interesting alternative procedure since it avoids Jacobian calculations.

**Keywords** Shape-memory alloys · Nonlinear dynamics · Lyapunov exponents · Tangent space · Cloned dynamics

## 1 Introduction

Dynamical systems employing shape-memory alloys (SMAs) have been studied since the 1990s, being characterized by rich and complex responses [1, 2]. The remarkable capacity to develop and recover high strain levels (or huge forces) and the intrinsic dissipation make SMAs to have a fast-growing technological interest that is represented by a scaling up of the number of articles published and patents issued for subsequent decades [3].

Dynamical analysis of SMA systems has different aspects that include distinct configurations and also the constitutive description of SMA thermomechanical behavior. Savi [4] presented a review article dealing with some dynamical issues related to SMA systems. Gholampour et al. [5] presented another overview of SMA dynamical applications.

As a prototype of the main characteristics of the SMA dynamical behavior, nonlinear dynamics of SMA oscillators is of concern in different investigations: Savi and Pacheco [6] employed a polynomial constitutive model to describe the SMA thermomechanical behavior; Lacarbonara et al. [7] employed the model proposed by Bernardini–Pence, investigating isothermal and non-isothermal conditions; Bernardini and Rega [8] employed a modified version of Bernardini-Pence's model also treating isothermal and anisothermal cases; Savi et al. [9] discussed nonlinear dynamics of SMA oscillators using the model proposed by Paiva et al. [10]; Bernardini and Rega [11, 12] investigated the heat exchange with the environment to understand the effect of the loading rate on the system's response and the influence of model parameters on the robustness and strength of

Technical Editor: Wallace Moreira Bessa, D.Sc.

✉ Pedro M. C. L. Pacheco
pedro.pacheco@cefet-rj.br

Alberto Paiva
albertopaiva@id.uff.br

Marcelo A. Savi
savi@mecanica.coppe.ufrj.br

1 Department of Mechanical Engineering, CEFET/RJ – Centro Federal de Educação Tecnológica Celso Suckow da Fonseca, Rio de Janeiro, RJ 20.271.110, Brazil

2 COPPE - Department of Mechanical Engineering, Center for Nonlinear Mechanics, Universidade Federal do Rio de Janeiro, P.O. Box 68.503, Rio de Janeiro, RJ 21.941.972, Brazil

3 Department of Mechanical Engineering, Universidade Federal Fluminense, Volta Redonda, RJ 27.255.250, Brazil

chaotic response. Bernardini and Rega [13] presented a general comparison of different kinds of constitutive models on the dynamical behavior of SMA oscillators. Du et al. [14], Rusinek et al. [15], and Weremczuk et al. [16] employed the harmonic balance method to evaluate SMA oscillators. Wang and Melnik [17] and Rajagopal et al. [18] are other examples of SMA oscillator investigations.

Besides, experimental works have been developed exploring the dynamical response of SMA systems. Lagoudas et al. [19] studied an SMA damping passive device and compared experimental results with numerical simulations employing the constitutive model proposed by Qidwai and Lagoudas [20]. Sitnikova et al. [21] performed a numerical experimental investigation of an impact oscillator with SMA constraint by varying the excitation frequency. Aguiar et al. [1] analyzed the vibration reduction exploiting either variations on temperature or vibration absorber techniques using a helicoidal SMA springs. Enemark et al. [22, 23] presented numerical experimental works regarding the dynamics of a pseudoelastic oscillator under free and forced vibration, varying temperature and pre-tension.

Dynamical applications using SMA elements are also explored in the literature. Santos and Savi [24] investigated the impacts of a one-degree-of-freedom oscillator (1-DOF) showing the influence of SMA elements. Silva et al. [25] investigated the nonlinear behavior of a Jeffcott rotor with SMA restoring elements on bearings. The dynamical behavior of a biomechanical device was treated by Rusinek et al. [26]. Costa and Savi [27] studied the dynamics of an SMA-pendulum system. Origami dynamics were investigated considering different configurations and folding patterns, as in Rodrigues et al. [28] and Fonseca et al. [29].

SMA structures are treated by different approaches including finite element method and reduced-order models. The two-bar truss is an interesting prototype structure largely employed for stability analysis. Savi et al. [30] and Savi and Nogueira [31] discussed the nonlinear dynamics of SMA two-bar truss using different constitutive models. The control of these kinds of structures is being analyzed by different references [32], including chaos control [33]. De Paula et al. [34] investigated aerospace large structures with SMA elements using reduced-order models. The use of SMA elements has a potential application on structures subjected to earthquakes [35]. Vignoli et al. [36] investigated the use of SMA hybrid composite materials applied to earthquake-resistant structures.

Nonlinear analysis requires special tools to achieve a proper diagnosis of the system behavior, especially chaos. Different types of invariants characterizing system dynamics are found in the literature for this aim. In general, the estimation of these invariants is split into two main approaches: based on mathematical models and based on time series analysis.

Kolmogorov entropy evaluates the sensitive dependence on initial conditions, measuring the degree of chaos inherent in a dynamical system. Correlation dimension measures the strangeness of an attractor, representing one of the most popular methods to estimates the attractor dimension. The 0–1 test is a diagnostic tool for nonlinear systems, laying on Brownian motion chain developed by Gottwald and Melbourne [37, 38] to distinguish chaotic from periodic behavior in deterministic systems. Bernardini and Litak [39] provided an overview of the main applications of the 0–1 test. Litak et al. [40], Bernardini et al. [41], and Savi et al. [42] employed the 0–1 test in SMA systems using time series obtained from numerical simulations. It should be pointed out that these tools are usually evaluated from time series analysis, being independent of the nature of the underlying dynamical system.

Lyapunov exponents arise as one of the most established and reliable tools to identify chaos. They have been extensively associated with the study of dynamical systems. In brief, the exponents are asymptotic measures that characterize the local average rate of growth (or shrinking) of small perturbations related to the orbits of the dynamical system. The estimation of Lyapunov exponents considers the exponential divergence of nearby trajectories in a phase space, which started close to each other. Several algorithms were developed based on this idea, and the calculations can be employed either from mathematical models or time series analysis.

Concerning time series analysis, the algorithms need to be robust due to unavoidable noise contamination. In this regard, the method developed by Kantz [43] presents low noise sensitivity. Besides, there are some alternatives such as Zeng et al. [44] and Rosenstein [45]. Concerning the approaches associated with mathematical equations, the algorithm developed by Wolf et al. [46] is the classical method to estimate Lyapunov exponents. It considers a trajectory in a tangent map and demands the calculation of the Jacobian matrix, a linearization of the equations of motion around a reference trajectory, which introduces difficulties for the application in some systems, such as SMA systems.

Recently, some alternative methods based on the perturbation method were proposed. Stefanski and Kapitaniak [47] proposed a novel approach to estimate the largest Lyapunov exponent using the perturbation method to discrete maps. Drabrowski [48] presented a new approach to calculate the largest Lyapunov exponent using the perturbation method showing results for a scheme of Duffing oscillators. Soriano et al. [49] proposed a new approach that can evaluate the Lyapunov spectrum employing initially perturbed clones of equations of motion, named *cloned dynamics*. The great advantage of this methodology lies on the cloned equations of motion, which replaces the linearized equations of the Wolf et al. method, being a Jacobian-free approach.

Specifically related to SMA systems, chaotic diagnosis considers different approaches. Savi and Braga [2] employed the classical algorithm due to Wolf et al. [46]. Machado et al. [50] proposed an alternative approach for the use of the algorithm due to Wolf et al. [46] in SMA systems with hysteresis based on the equivalent linear dissipation. On the other hand, Litak et al. [40], Bernardini et al. [41], and Savi et al. [42] employed the 0–1 test in SMA systems using time series obtained from numerical simulations. Recently, Syta et al. [51] presented a comparison between the largest Lyapunov exponent, 0–1 test, and recurrence plots [52] utilizing time series analysis showing coherent results for all approaches.

This work deals with the analysis of Lyapunov exponents of SMA systems using both the cloned dynamics algorithm [49] and the tangent map algorithm [46]. The main contribution is to evaluate the capability of the cloned dynamics method through a comparison with the classical tangent map method, validating its use for SMA systems. Different kinds of response are of concern, establishing a general validation of the Jacobian-free approach. One- and two-degree-of-freedom systems are investigated, evaluating different kinds of responses. A polynomial constitutive model is employed to describe the thermomechanical behavior of SMAs [53]. This analysis can be understood as a proof of concept, being possible to be extended for other models that present a better description of the hysteretic behavior of the SMA systems.

The paper is organized as follows: Section 2 discusses the Lyapunov exponents, presenting the tangent map and the cloned dynamics methods. Section 3 is devoted to the SMA dynamical model considering 1-DOF and 2-DOF models. Section 4 presents the methodology for the numerical simulations, results, and discussions about both SMA oscillators and *Lyapunov* exponents' calculations. Finally, Sect. 5 presents the final remarks and conclusions.

## 2 Lyapunov spectrum

Lyapunov exponents estimate the sensitivity to initial conditions by evaluating the local divergence of nearby orbits. The idea is to monitor the distance between a reference orbit and its neighbor orbits, while the system evolves through time. If the measured distance increases, there is a local divergence that characterizes chaos. Chaotic response is, therefore, associated with one positive value, which represents a divergent direction. The existence of a positive Lyapunov exponent is related to the horseshoe transformation that characterizes chaos. If all measures decrease, there is a local convergence, characterizing periodic behavior.

In order to present the main idea about Lyapunov exponents calculation, consider an $n$-dimensional dynamical system of the form:

$$\dot{x} = \frac{\mathrm{d}x}{\mathrm{d}t} = g(x,t) \tag{1}$$

The idea is to monitor perturbations around a reference orbit, which can be represented by an $n$-dimensional sphere of initial conditions centered at the reference orbit. Therefore, it is necessary to monitor this sphere, which can be done by considering the evolution from an initial state, $d_0$, through time evolution as follows:

$$\mathrm{d}(t) = \mathrm{d}_0 e^{\lambda(t)} \tag{2}$$

where $\lambda$ represents the spectrum of Lyapunov exponent, being associated with the system dimension.

The sign of the Lyapunov exponents provides a qualitative picture of the system dynamics. A negative value is associated with a contraction direction of the sphere, while a positive sign is related to an expansion direction. Since chaotic behavior is characterized by the existence of the horseshoe transformation, these exponents illustrate the transformation of a sphere into an ellipsoid, as shown in Fig. 1.

There are several algorithms to calculate Lyapunov exponents. Here, two different approaches are treated: the classical algorithm due to Wolf et al. [46], classified as a tangent map method; and the cloned dynamics approach [49]. Basically, both methods monitor the evolution of the nearby orbits considering an extension of the original system. The essential difference is the definition of this extension.

Since chaotic situations are related to a local exponential divergence of nearby orbits, it is necessary to evaluate the average of this divergence considered in different points of the trajectory. Figure 2 presents a schematic representation of the system evolution and the algorithm strategy. Hence, initial conditions of the perturbed orbits are changed for each time step, establishing the following definition:

$$\lambda = \frac{1}{t - t_0} \sum_{k=0}^{n} \log\left(\frac{\mathrm{d}\left(t_k\right)}{\mathrm{d}_0\left(t_{k-1}\right)}\right). \tag{3}$$

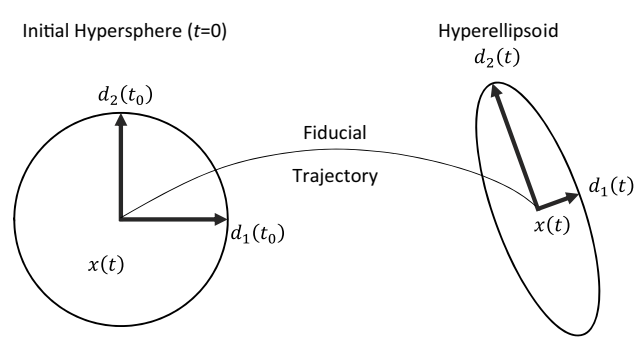


**Fig. 1** Lyapunov exponents—hypersphere evolving to an hyperellipsoid

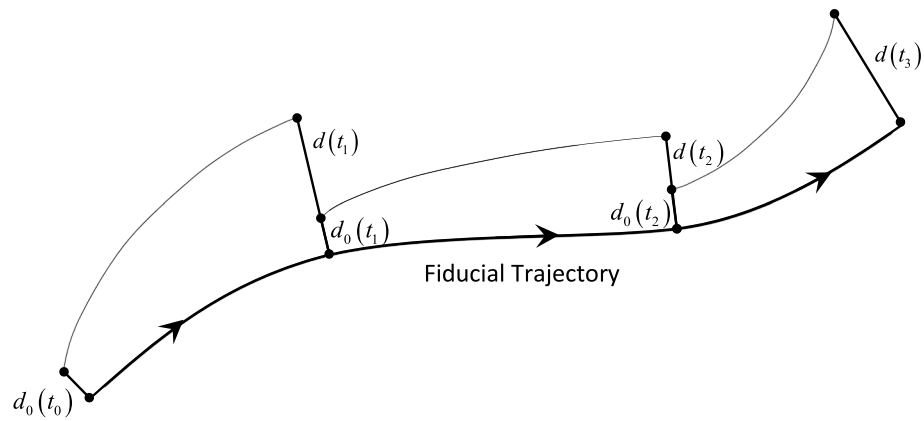


**Fig. 2** Fiducial trajectory and perturbed trajectory

### 2.1 Tangent map approach: Wolf et al. [46]

The classical, well-established approach to estimate Lyapunov exponents is due to Wolf et al. [46], being classified as a tangent map method. The main idea is to monitor the nearby orbit considering an extension on a tangent map space, using a linearized version of the equations of motion:

$$\dot{\eta} = A\eta \tag{4}$$

where $A = Df\left(\phi\left(x_0, t\right), t\right)$ is the Jacobian matrix and the variable $\eta$ represents the perturbed orbits.

In order to deal with all exponent spectrum, an orthonormal basis related to each component of the vector $\eta$ must be evaluated, which is done by the Gram–Schmidt reorthonormalization process. Therefore, the distance $d_0$ is restarted to each time step, being defined as follows:

$$d_0\left(t_{k-1}\right) = d_0^{\mathrm{GS}} \tag{5}$$

where $d_0^{\mathrm{GS}}$ is the perturbation norm calculated from the Gram–Schmidt normalization based on the evolution from the previous time step, $d_0\left(t_{k-1}\right)$.

### 2.2 Cloned dynamics approach: Soriano et al. [49]

The cloned dynamics approach was proposed by Soriano et al. [49] to estimate Lyapunov exponents following the same idea of the one proposed by Wolf et al. [46]. The essential difference is that the new approach employs clones of the original dynamical system as the extension of the dynamical system. In this regard, the perturbed orbit is provided by the cloned system instead of a linear system extension. In this way, the cloned dynamics approach avoids the calculation of the Jacobian matrix.

The initial sphere is assigned by a perturbation, $\Lambda$ [49]. Afterward, the Gram–Schmidt reorthonormalization process is applied in order to restart the perturbation but is still based on the initial perturbation. Therefore, the cloned system receives new perturbed initial conditions in relation to the fiducial trajectory along the orthonormal basis:

$$d_0\left(t_{k-1}\right) = \Lambda d_0^{\mathrm{GS}} \tag{6}$$

Note that the difference between this approach and the classical one is a rescale of the Gram–Schmidt using the parameter $\Lambda$. It should also be pointed out that initial condition related to the perturbation is defined just by the parameter $\Lambda$.

The cloned dynamics approach is similar to the classical one but does not require a linearization, using the same equations of motion instead. Besides, it should be pointed out that this approach needs the definition of the perturbation parameter, $\Lambda$, which should be chosen appropriately.

## 3 SMA dynamical models

This section is devoted to present the physical model of the SMA oscillators and their respective mathematical formulation. The first section presents the constitutive model employed to describe the thermomechanical behavior of SMA. Afterward, two different SMA oscillators are treated: one-degree of freedom (1-DOF) and two-degree of freedom (2-DOF).

### 3.1 Constitutive model

The thermomechanical behavior of SMAs can be described by a polynomial constitutive model proposed by Falk [53]. Basically, a Helmholtz free energy is defined as a function of observable state variables, temperature, $T$, and strain, $\varepsilon$, in order to represent the stability characteristics of microscopic phases, austenite and martensite. Considering a temperature-dependent sixth-order strain polynomial in such a way that for low temperatures where martensite is stable at a stress-free state, there are two minima representing the two martensitic variants (tension-induced and

compression-induced). For intermediate temperature, the potential presents three minima indicating that both martensitic phases and austenite can be stable. For high temperatures, the potential presents only one minimum, indicating that austenite is the only stable in a stress-free state. Based on that, the stress–strain–temperature relation is given by Savi and Pacheco [6]:

$$\rho\psi(\varepsilon,T)=\frac{\alpha\left(T-T_{\mathrm{M}}\right)}{2}\varepsilon^2-\frac{\beta}{4}\varepsilon^4+\frac{\gamma}{6}\varepsilon^6 \tag{7}$$

where $\alpha$, $\beta$ and $\gamma$ are material parameters, while $T_{\mathrm{M}}$ is the temperature below which martensitic phase is stable.

By deriving the Helmholtz free energy potential with respect to strain, the constitutive equation is obtained represented by the following stress–strain–temperature relation:

$$\sigma(\varepsilon,T)=\alpha\left(T-T_{\mathrm{M}}\right)\varepsilon-\beta\varepsilon^3+\gamma\varepsilon^5 \tag{8}$$

where $\sigma$ represents the stress.

The main advantage of this model is its simplicity, but it does not describe dissipation due to the hysteresis loop. This drawback can be overcome by combining a linear viscous damper in parallel with the shape-memory alloy element. Dynamical behavior of SMA system is treated considering oscillators, modeled in the sequence.

### 3.2 1-DOF oscillator

Consider a 1-DOF oscillator presented in Fig. 3, composed of an inertial element, with mass $m$, connected to an SMA element, described by the polynomial model (which exerts a restoring force $F_{\mathrm{SMA}}=\sigma A$), and a linear viscous damping element with coefficient $c$, subjected to an external harmonic force, $F(t)=F_0\cos(\Omega\, t)$. By assuming a displacement along $x$-direction denoted by $u(t)$, and considering that the strain is $\varepsilon=u/L$, where $L$ is the length of the SMA element, the following equation of motion is obtained:

$$m\ddot{u}+c\dot{u}+\alpha\frac{A}{L}\left(T-T_M\right)u-\beta A\left(\frac{u}{L}\right)^3+\gamma A\left(\frac{u}{L}\right)^5=F_0\cos\left(\Omega t\right) \tag{9}$$

In order to obtain a dimensionless set of ordinary differential equations, new variables are created. Dimensionless time is defined as $\tau=t\omega$ where $\omega=\sqrt{\frac{\alpha A T_{\mathrm{M}}}{mL}}$ is a reference frequency. The dimensionless displacement is expressed by $U=u/L$; dimensionless temperature is given by $\theta=\frac{T}{T_{\mathrm{M}}}$. Therefore, the following dimensionless equation of motion is obtained:

$$U_1''+\xi U'+\bar{\alpha}(\theta-1)U-\bar{\beta}U^3+\bar{\gamma}_1U^5=f\cos\left(\tau\varpi\right) \tag{10}$$

where the following parameters are employed:

$$f=\frac{F_0}{mL\omega^2};\quad \varpi=\frac{\Omega}{\omega};\quad \xi=\frac{c}{m\omega};\quad \bar{\alpha}=\frac{\alpha A T_{\mathrm{M}}}{mL\omega^2};\quad \theta=\frac{T}{T_{\mathrm{M}}};\quad \bar{\beta}=\frac{\beta A}{mL\omega^2};\quad \bar{\gamma}=\frac{\gamma A}{mL\omega^2}. \tag{11}$$

### 3.3 2-DOF oscillator

Consider a 2-DOF SMA oscillator presented in Fig. 4. The mass $m_1$ is connected to two identical damping elements—$c_1$ and $c_2$—and two SMA elements—$SMA_1$ and $SMA_2$. The mass $m_2$ is connected to four elements as well, a pair of SMA elements—$SMA_2$ and $SMA_3$—and a pair of damping elements—$c_2$ and $c_3$.

Both masses move in the $x$-direction, and the displacements of each mass are represented by $u_1(t)$ and $u_2(t)$, respectively. An external harmonic excitation, $F(t)$, is applied to the mass $m_1$. Based on Newton's law, the equations of motion are given by:

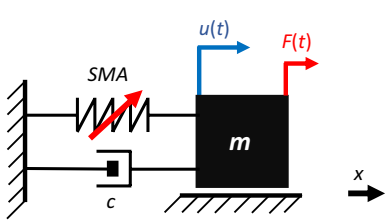


**Fig. 3** Physical model of 1-DOF oscillator

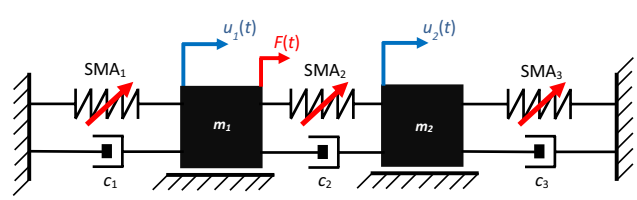


**Fig. 4** Physical model of 2-DOF oscillator

$$\begin{cases} m\ddot{u}_1 + \left(c_1\dot{u}_1 + \alpha\frac{A}{L}(T-T_{\mathrm{M}})u_1 - \beta A\left(\frac{u_1}{L}\right)^3 + \gamma A\left(\frac{u_1}{L}\right)^5\right) \\ \quad -\left(c_2(\dot{u}_2-\dot{u}_1) + \alpha\frac{A}{L}(T-T_{\mathrm{M}})(u_2-u_1) - \beta A\left(\frac{u_2-u_1}{L}\right)^3 + \gamma A\left(\frac{u_2-u_1}{L}\right)^5\right) = F_0\cos(\Omega t) \\ m\ddot{u}_2 + \left(c_2(\dot{u}_2-\dot{u}_1) + \alpha\frac{A}{L}(T-T_{\mathrm{M}})(u_2-u_1) - \beta A\left(\frac{u_2-u_1}{L}\right)^3 + \gamma A\left(\frac{u_2-u_1}{L}\right)^5\right) \\ \quad +\left(c_3\dot{u}_2 + \alpha\frac{A}{L}(T-T_{\mathrm{M}})u_2 - \beta A\left(\frac{u_2}{L}\right)^3 + \gamma A\left(\frac{u_2}{L}\right)^5\right) = 0 \end{cases} \tag{12}$$

By assuming a similar approach adopted for the 1-DOF oscillator using dimensionless variables, the following equations can be written:

$$\begin{cases} U_1'' + \xi_1 U_1' - \xi_2 U_2' + \bar{\alpha}(\theta_1-1)U_1 - \bar{\beta}U_1^3 + \bar{\gamma}U_1^5 - \bar{\alpha}(U_2-U_1)(\theta_2-1) \\ \quad +\bar{\beta}(U_2-U_1)^3 - \bar{\gamma}(U_2-U_1)^5 = f\cos(\varpi t) \\ U_2'' = \xi_3 U_1' - \xi_4 U_2' + \bar{\alpha}(\theta_2-1)(U_2-U_1) - \bar{\beta}(U_2-U_1)^3 + \bar{\gamma}(U_2-U_1)^5 \\ \quad +\bar{\alpha}(\theta_3-1)U_2 - \bar{\beta}U_2^3 + \bar{\gamma}U_2^5 \end{cases} \tag{13}$$

where the new dimensionless parameters are given by:

$$\begin{aligned} &f = \frac{F_0}{mL\omega^2};\quad \varpi = \frac{\Omega}{\omega};\quad \xi_1 = \frac{c_1+c_2}{m\omega};\quad \xi_2 = \frac{c_2}{m\omega};\quad \xi_3 = \frac{c_2}{m\omega};\quad \xi_4 = \frac{c_2+c_3}{m\omega}; \\ &\bar{\alpha} = \frac{\alpha A T_{\mathrm{M}}}{mL\omega^2};\quad \bar{\beta} = \frac{\beta A}{mL\omega^2};\quad \bar{\gamma} = \frac{\gamma A}{mL\omega^2};\quad \theta_1 = \theta_2 = \theta_3 = \frac{T}{T_{\mathrm{M}}}. \end{aligned} \tag{14}$$

## 4 Numerical simulations

The fourth-order Runge–Kutta method is employed to perform numerical simulations. Time step, $\Delta t$, is linked to the forcing frequency, $\varpi$, and the number of divisions per period, $n_d$, leading to the time step: $\Delta t = 2\pi/\omega n_d$. The number of periods simulated must be enough to allow the system to reach a steady-state condition. A transient dynamical response is considered for the first 29,000 periods of a total of 30,000 periods, and therefore, the steady-state condition is analyzed considering the last 1000 periods.

Bifurcation diagrams are employed to evaluate the global system response. The dimensionless force amplitude is chosen as a control parameter. Besides, Lyapunov exponents are evaluated together with the bifurcation diagram, allowing a proper comprehension of the system dynamics. It is worth mentioning that Lyapunov exponents are calculated comparing tangent map and cloned dynamics, in order to check the compatibility between results.

Numerical results consider SMA oscillators, both 1-DOF and 2-DOF. The dimensionless parameters values are displayed in Table 1, being related to typical values of NiTi [28]:

**Table 1** Oscillator parameters

| $\xi$ | $\bar{\alpha}$ | $\bar{\beta}$ | $\bar{\gamma}$ |
|---|---|---|---|
| 0.1 | 1 | $1.3\times10^3$ | $4.7\times10^5$ |

Table 2 presents parameters related to temperature and forcing frequencies. The analysis performed for 1-DOF oscillator considers three different temperature levels and

**Table 2** Temperatures and excitation frequencies analyzed

| Analysis | 1-DOF | | | | | | | | | 2-DOF | | |
|---|---|---|---|---|---|---|---|---|---|---|---|---|
| $\theta$ | 0.7 | | | 1.5 | | | 2.0 | | | 0.7 | 1.5 | 2.0 |
| $\varpi$ | 0.1 | 1.0 | 2.0 | 0.1 | 1.0 | 2.0 | 0.1 | 1.0 | 2.0 | 1.0 | | |

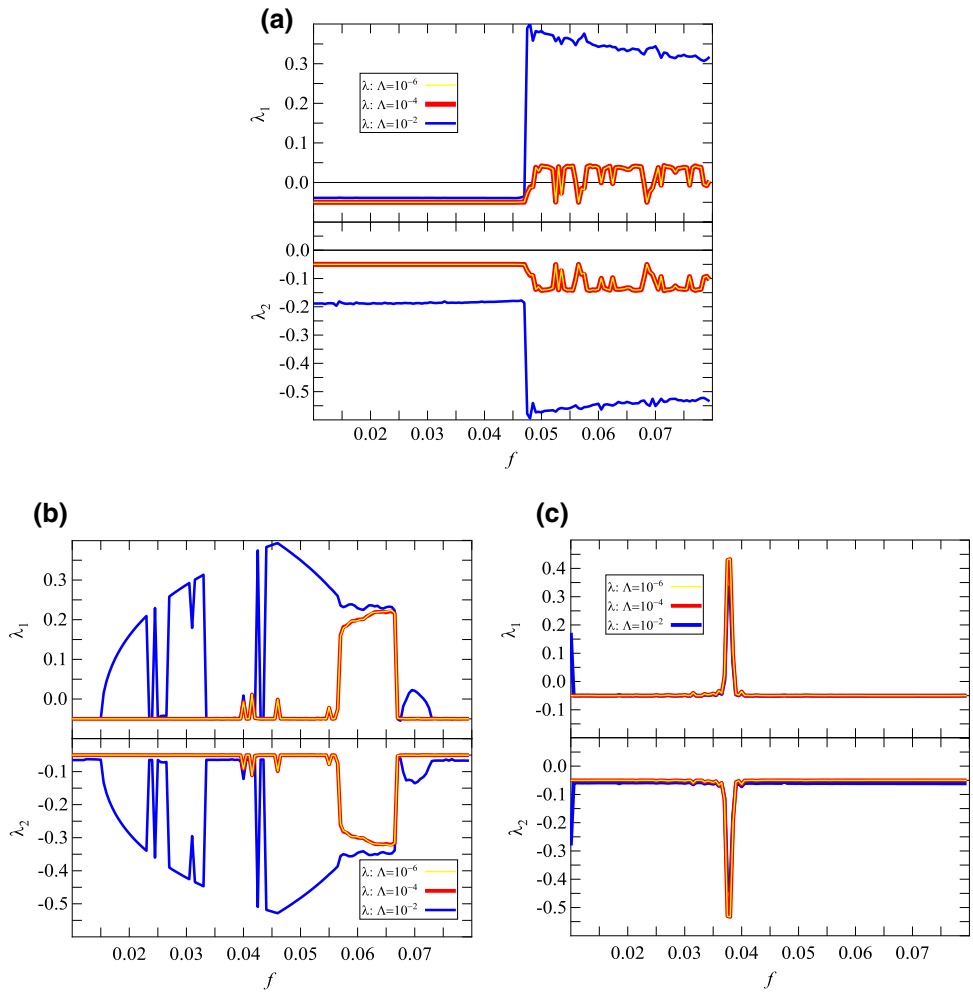


**Fig. 5** Analysis of perturbation parameter of the cloned dynamics approach for a 1-DOF oscillator considering different perturbations ($\Lambda = 10^{-2}$, $\Lambda = 10^{-3}$, $\Lambda = 10^{-4}$, $\Lambda = 10^{-6}$) at low level temperature and three different frequencies: **a** $\varpi = 0.1$; **b** $\varpi = 1$; **c** $\varpi = 2$

three frequency values: low frequency, $\varpi = 0.1$; intermediate frequency, $\varpi = 1$; high frequency, $\varpi = 2$. On the other hand, the investigation for 2-DOF oscillator considers only one frequency value and three different temperature levels: low temperature level, $\theta = 0.7 < T_M$; intermediate temperature level, $\theta = 1.5 > T_M$; and high temperature level, $\theta = 2.0 > T_M$.

### 4.1 Cloned dynamics perturbation parameter

The cloned dynamics approach is a Jacobian-free approach, but needs the definition of an initial perturbation. Therefore, the starting point for the dynamical analysis is the definition of a proper value for this parameter. This section investigates the influence of this choice on the estimation of the Lyapunov exponents, defining a strategy for its identification based on convergence analysis.

Initially, the 1-DOF system is of concern. A diagram with Lyapunov exponents after stabilization is built with a slow quasistatic variation of the forcing amplitude. Three different frequencies are considered for a low-temperature case ($\theta = 0.7$). Three different perturbation parameter values are of concern: $\Lambda = 10^{-2}$, $\Lambda = 10^{-4}$, and $\Lambda = 10^{-6}$. Figure 5 presents results for the Lyapunov exponents evaluated with cloned dynamics with different perturbations. Note that results are the same considering $\Lambda = 10^{-4}$ and $\Lambda = 10^{-6}$. On the other hand, it should be noticed that $\Lambda = 10^{-2}$ presents results that differ from the previous ones. This points to a procedure convergence with respect to the perturbation. Based on that, it is possible to conclude that perturbations less than $\Lambda = 10^{-4}$ can be employed for the cloned dynamics approach. The same analysis can be extended for the other exponents of the spectrum. It should be pointed out that an unproper choice of these parameters can provide results that can furnish wrong results, pointing to a wrong sign of the exponents, introducing difficulties to chaos diagnosis.

The 2-DOF oscillator is now of concern. The same analysis is developed considering bifurcation diagrams for three distinct temperature levels with respect to forcing amplitude, Fig. 6. Lyapunov exponents are estimated

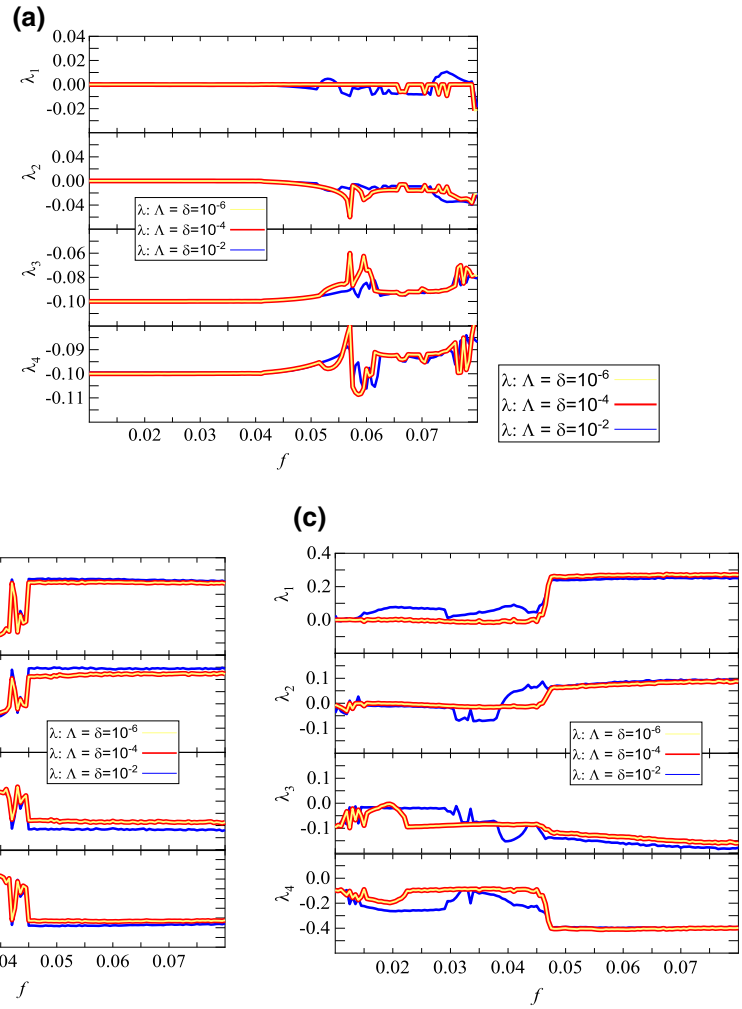


**Fig. 6** Analysis of perturbation parameter of the cloned dynamics approach for a 2-DOF oscillator considering different perturbations ($\Lambda = 10^{-2}$, $\Lambda = 10^{-4}$, $\Lambda = 10^{-6}$) and three temperatures: **a** $\theta = 0.7$; **b** $\theta = 1.5$; **c** $\theta = 2$

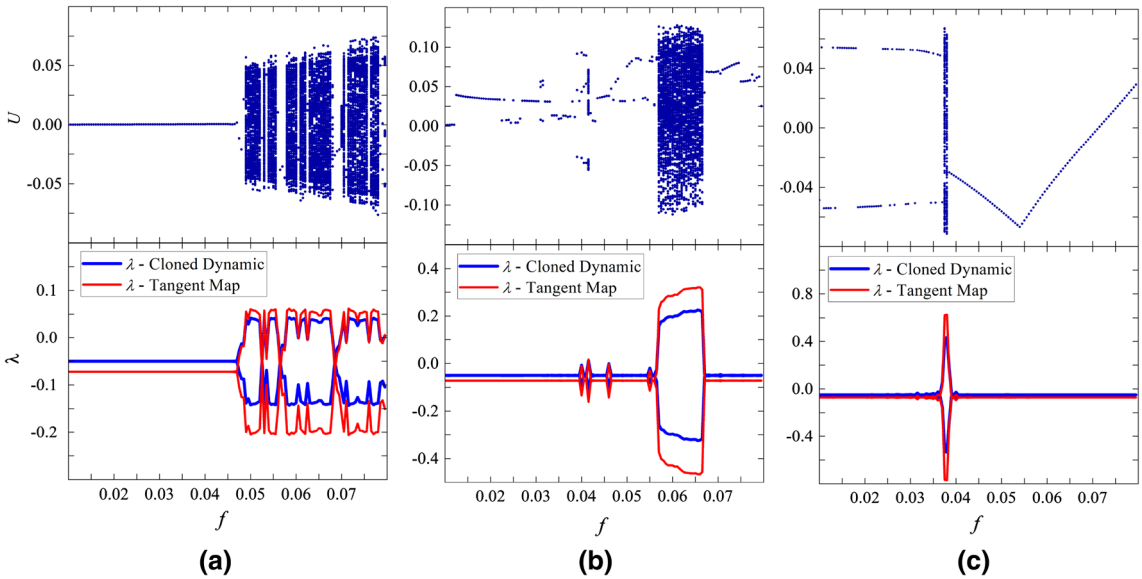


**Fig. 7** Bifurcation diagrams and Lyapunov exponents varying forcing amplitude for temperature $\theta = 0.7$ and different frequencies: **a** $\varpi = 0.1$; **b** $\varpi = 1$; **c** $\varpi = 2$

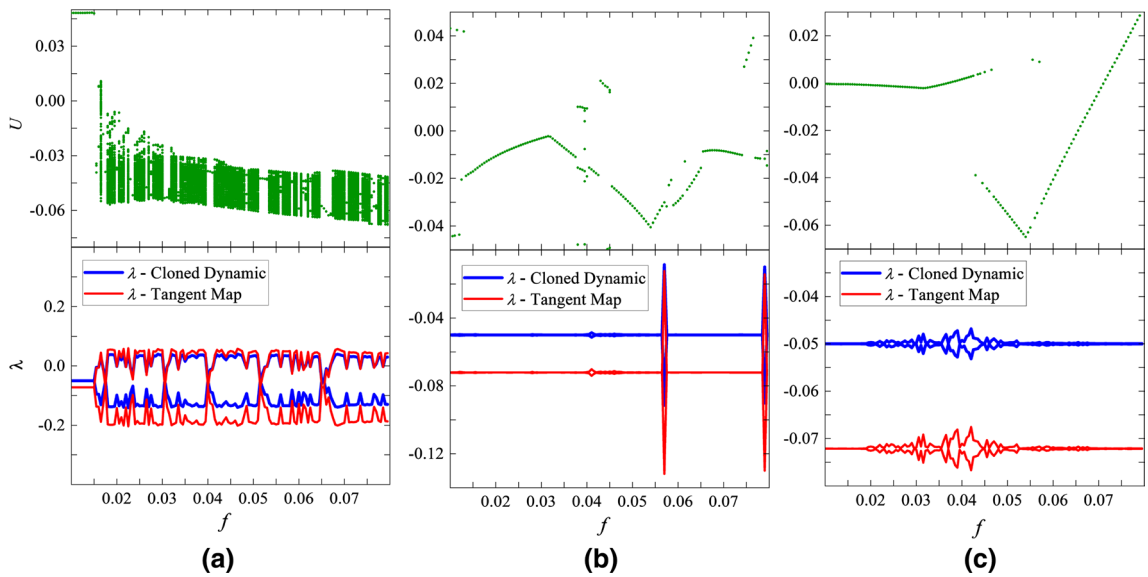


**Fig. 8** Bifurcation diagrams varying forcing amplitude correlated with the *Lyapunov* exponents for temperature equal to $\theta = 1.5$ and frequency: **a** $\varpi = 0.1$; **b** $\varpi = 1$; **c** $\varpi = 2$

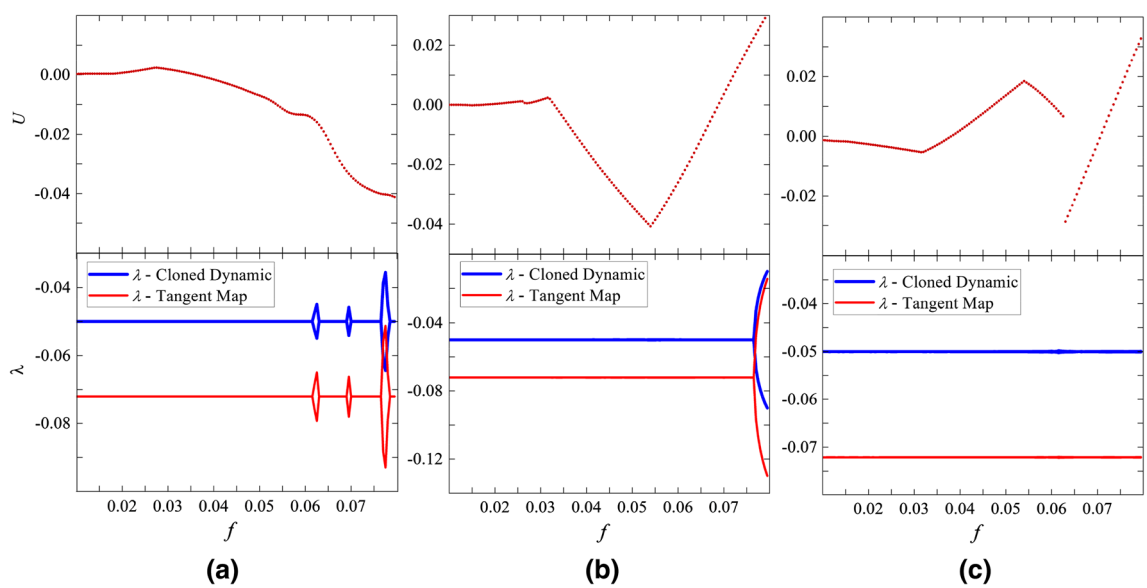


**Fig. 9** Bifurcation diagrams varying forcing amplitude correlated with the *Lyapunov* exponents for temperature equal to $\theta = 2$ and frequency: **a** $\varpi = 0.1$; **b** $\varpi = 1$; **c** $\varpi = 2$

for three different perturbations: $\Lambda = 10^{-2}$, $\Lambda = 10^{-4}$ and $\Lambda = 10^{-6}$. Once again, results converge with respect to the perturbation parameter, and the value of $\Lambda = 10^{-4}$ is the best choice. Besides, wrong results can be estimated with the unproper choice of $\Lambda$.

From this point on, the cloned dynamics approach uses the perturbation parameter $\Lambda = 10^{-4}$.

### 4.2 1-DOF oscillator dynamical analysis

The nonlinear dynamics of the 1-DOF oscillator is of concern. The essential point is to establish a comparison between both approaches to estimate Lyapunov exponents. Figure 7 presents bifurcation diagrams, together with Lyapunov exponents calculated with tangent map and cloned dynamics approaches. Forcing frequencies $\varpi = 0.1$ and $\varpi = 2$ are presented, respectively, in Fig. 7a–c, considering low temperature level.

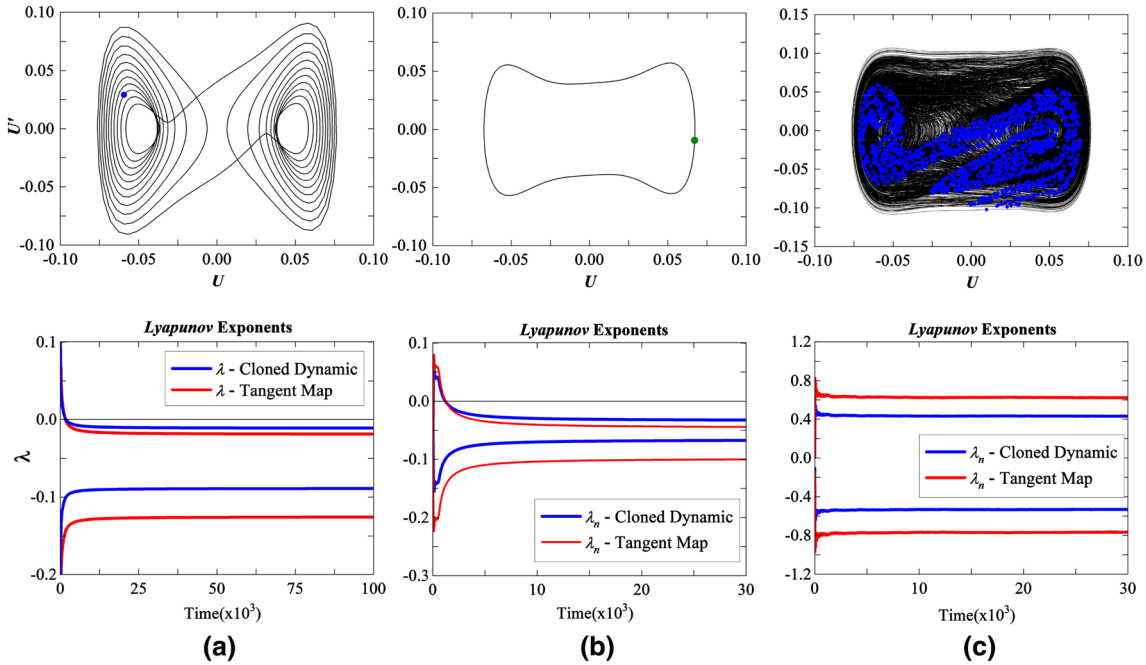


**Fig. 10** Phase space combined with *Poincaré* map and a comparison between *Lyapunov* exponents along the time obtained using the cloned dynamic and tangent map approaches: **a** $\theta=0.7$, $\varpi=0.1$, $f=0.0480$; **b** $\theta=1.5$, $\varpi=0.1$, $f=0.0235$; **c** $\theta=0.7$, $\varpi=2$, $f=0.0380$

Responses have a significant difference for each frequency. Figure 7a presents a wide range of period-1 response—from $f=0.01$ to $f=0.049$ confirmed by negative Lyapunov exponents. The system response becomes chaotic interspersed with some periodic windows. Chaotic responses are assured by positive value of Lyapunov exponents. Figure 7b shows that the increase in the forcing frequency causes a reduction of the aperiodic band and some dynamical jumps. The chaotic response between $f=0.057$ and $f=0.0665$ is confirmed by both approaches to calculate the Lyapunov exponents. Figure 7c exhibits a reduction of the chaotic range if compared to Fig. 7a, b. Besides, the dynamical jumps now occur only before the periodic window. Regarding Lyapunov exponents, both methods confirm that the non-periodic behavior is chaotic. It should be highlighted that both methods present similar results for all cases.

Figure 8 shows results for intermediate temperature level ($\theta=1.5$) and the three forcing frequencies. Figure 8a refers to the lowest forcing frequency, $\varpi=0.1$, presenting a small range of periodicity-1, from $f=0.01$ to $f=0.015$ with negative exponents. Afterward, there are regions of non-periodic responses and periodic windows. Note that non-periodic responses are related to quasiperiodic and chaotic behaviors, captured by null and positive Lyapunov exponents. Figure 8b, c exhibit periodic responses for both cases, which can also be confirmed by the Lyapunov exponents, through both methods. It should be highlighted a reduction of the dynamical jumps.

Figure 9 presents high-temperature behavior of the 1-DOF SMA oscillator. Under this condition, the system has a single well behavior being expected that it presents a periodic-1 behavior overall range of the forcing amplitude. Based on that, all Lyapunov exponents present negative values. These results show that both algorithms have the same behavior, capturing the general behavior of the oscillator under different conditions. The small discrepancies observed do not affect the qualitative behavior defined by the signs of the exponents. In other words, the results of both methods offer the same conclusion about the kind of response.

Results for some specific set of parameters are now evaluated in order to observe the estimated Lyapunov exponents calculated based on both approaches. The idea is to consider different kinds of responses. Figure 10 exhibits a phase space with a Poincaré map and the Lyapunov exponent time history considering cloned dynamics and tangent maps, for low and intermediate temperatures. Figure 10a, b shows periodic behavior attested by two negative Lyapunov exponents calculated by both approaches. Despite the quantitative discrepancy between them, all responses are qualitatively the same. It is also noticeable that the convergence period is similar for both cases. Figure 10c presents a non-periodic response associated with chaos since Lyapunov exponents have a maximum positive value. Both approaches present the same qualitative response with a similar convergence time and small quantitative discrepancy.

### 4.3 2-DOF Oscillator Dynamical Analysis

A 2-DOF SMA oscillator is now of concern. Figure 11 shows bifurcation diagrams together with Lyapunov exponents under the variation of forcing amplitude, considering a forcing frequency of $\varpi = 1$. The main difference from 1-DOF to 2-DOF SMA system is the possibility of the Lyapunov exponents which present two positive exponents, characterizing a hyperchaotic behavior where at least two directions diverge.

Figure 11a presents a low-temperature case. Initially, forcing amplitudes present periodic responses. When the

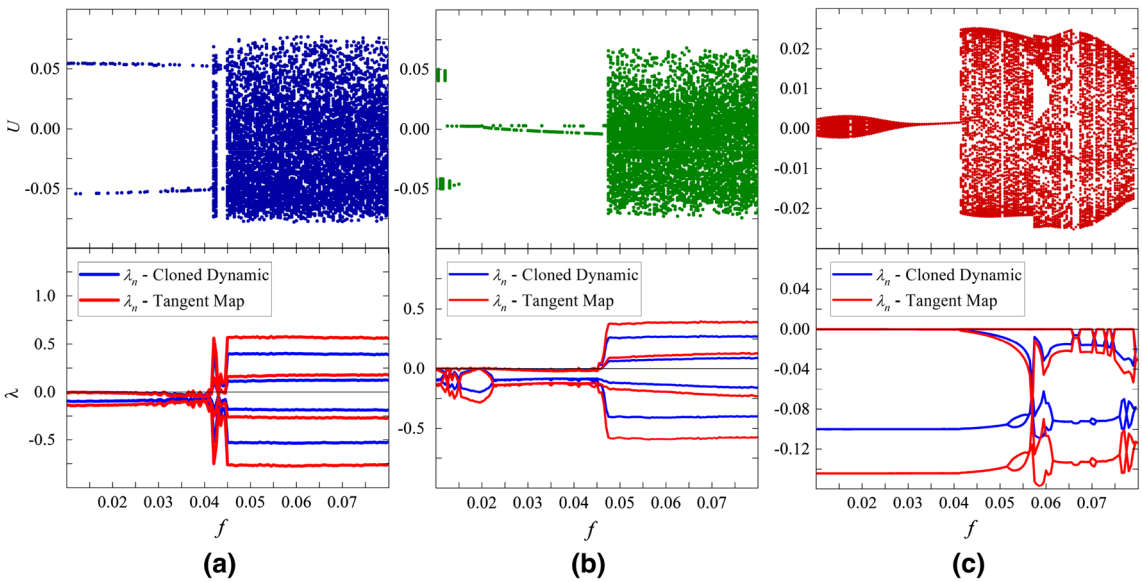


**Fig. 11** Bifurcation diagrams varying forcing amplitude correlated with the *Lyapunov* exponents for frequency equal to $\varpi = 1$ and temperature: **a** $\theta = 0.7$; **b** $\theta = 1.5$; **c** $\theta = 2$

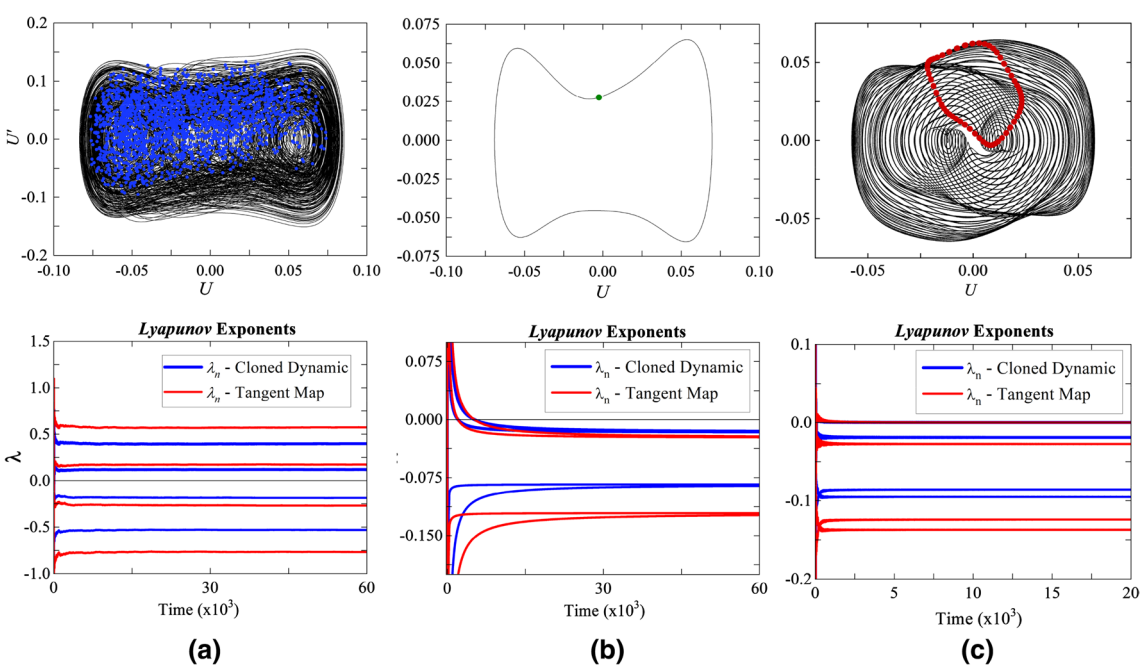


**Fig. 12** Phase space combined with *Poincaré* map and a comparison between *Lyapunov* exponents along the time obtained using the cloned dynamic and tangent map approaches: **a** $\theta = 0.7, f = 0.060$; **b** $\theta = 1.5, f = 0.037$; **b** $\theta = 2, f = 0.058$

forcing amplitude is $f = 0.0405$, there is a small window presenting chaotic and hyperchaotic behavior, succeeded by a periodic response at $f = 0.043$ and a chaotic one at $f = 0.0445$. After that, the response is hyperchaotic. The hyperchaos is correctly recognized by both approaches, and, once again, there is a small quantitative discrepancy. Figure 11b presents the system response for intermediate temperature, showing similar results. The nature of the response is predominantly non-periodic, varying from quasiperiodic response to hyperchaos after $f = 0.0445$, highlighting that there are some periodic and chaotic responses interleaved in the quasiperiodic responses. Lyapunov exponents measured through both approaches indicate the same behavior for all points evaluated. Figure 11c considers high-temperature behavior, and results are essentially quasiperiodic, except for small periodic windows after $f = 0.058$. Once again, both methodologies present similar results.

Different kinds of behaviors are now of concern. Figure 12a shows a non-periodic response represented by a dense phase space. Figure 12b presents a periodic orbit. Figure 12c presents another dense phase space with a Poincaré map associated with a closed form.

Figure 12a presents a dense phase state, and the Poincaré map displays a distorted cloud of points without presenting the characteristics of a strange attractor, or a circle/torus form, which would represent a quasiperiodic response. This kind of aspect usually appears on hyperchaotic responses. The distorted cloud of points marked by the Poincaré map is a consequence of the expansion occurring in two directions, instead of just one, which means two directions diverging or expanding. For the case presented in Fig. 12b, both approaches to estimate the *Lyapunov* exponents attest the presence of hyperchaotic behavior. On the other hand, a single orbit with one point marked on the Poincaré map and all four exponents negative estimated by tangent map and cloned dynamic approaches attest the periodic behavior. Figure 12c displays a closed form on the Poincaré map, and the highest Lyapunov exponent is zero, confirming a quasiperiodic behavior. It is essential to highlight that even on increasing the complexity of the system, the cloned dynamic approach presents similar results and similar convergence period.

## 5 Conclusions

This work deals with the estimation of Lyapunov exponents on shape-memory alloy systems. The idea is to investigate the Jacobian-free cloned dynamics approach, proposed by Soriano et al. [49], establishing a comparison with the classical tangent map approach, proposed by Wolf et al. [46], defining its validation for different kinds of response. SMA oscillators with 1-DOF and 2-DOF are investigated employing a polynomial constitutive model to describe the thermomechanical behavior of SMAs. Numerical simulations show that both systems present a wide variety of responses, including chaos, hyperchaos, and quasiperiodic responses. Cloned dynamics approach avoids the calculation of the Jacobian matrix, but needs the determination of a perturbation parameter. An approach based on a convergence analysis is proposed to define the best choice for this parameter, which makes its determination feasible for diagnosis perspective. Results point that the cloned dynamics approach can be used to identify complex dynamical behavior of shape-memory alloy systems with the advantage of a Jacobian-free approach. Besides, this investigation can be understood as a proof of concept in the sense that it can be extrapolated to SMA systems described by other constitutive equations.

**Acknowledgements** The authors would like to acknowledge the support of the Brazilian Research Agencies CNPq, FAPERJ and CAPES.

## References

1. Aguiar RAA, Savi MA, Pacheco PMCL (2012) Experimental investigation of vibration reduction using shape memory alloys. J Intell Mater Syst Struct 24(2):247–261
2. Savi MA, Braga AMB (1993) Chaotic vibrations of an oscillator with shape memory. J Braz Soc Mech Sci Eng 15(1):1–20
3. Jani JM, Leary M, Subic A, Gibson MA (2014) A review of shape memory alloy research, applications and opportunities. Mater Des 1980–2015(56):1078–1113
4. Savi MA (2015) Nonlinear dynamics and chaos in shape memory alloy systems. Int J Nonlinear Mech 70:2–19
5. Gholampour AA, Ghassemieh M, Kiani J (2014) State of the art in nonlinear dynamic analysis of smart structures with SMA members. Int J Eng Sci 75:108–117
6. Savi MA, Pacheco PMCL (2002) Chaos and hyperchaos in shape memory systems. Int J Bifurc Chaos 12(03):645–657
7. Lacarbonara W, Bernardini D, Vestroni F (2004) Nonlinear thermomechanical oscillations of shape-memory devices. Int J Solids Struct 41(5–6):1209–1234
8. Bernardini D, Rega G (2005) Thermomechanical modeling nonlinear dynamics and chaos in shape memory oscillators. Math Comput Modem Dyn Syst 11:291–314
9. Savi MA, Sá MAN, Pacheco PMCL (2008) Tensile-compressive asymmetry influence on shape memory alloy system dynamics. Chaos Solitons Fractals 36:828–842
10. Paiva A, Savi MA, Braga MA, Pacheco PMCL (2005) A constitutive model for shape memory alloys considering tensile-compressive assymetry and plasticity. Int J Solid Struct 42(11–12):3439–3457
11. Bernardini D, Rega G (2011) Chaos robustness and strength in thermomechanical shape memory oscillators. Part I: a predictive theoretical framework for the pseudoelastic behavior. Int J Bifurc Chaos 21(10):2769–2782
12. Bernardini D, Rega G (2011) Chaos robustness and strength in thermomechanical shape memory oscillators. Part II: numerical and theoretical evaluation. Int J Bifurc Chaos 21(10):2783–2800
13. Bernardini D, Rega G (2017) Evaluation of different SMA models performances in the nonlinear dynamics of pseudoelastic

oscillators via comprehensive modeling framework. Int J Mech Sci 130:458–475
14. Du H, He X, Wang L, Melnik R (2020) Analysis of shape memory alloy vibrator using harmonic balance method. Appl Phys A 126(7):1–9
15. Rusinek R, Rekas J, Kecik K (2019) Vibration analysis of a shape memory oscillator by harmonic balance method verified numerically. Int J Bifurc Chaos 29(3):1–14
16. Weremczuk A, Rekas J, Rusinek R (2019) Low- and high-temperature primary resonance in shape memory oscillator observed by multiple time scales and harmonic balance method. J Comput Nonlinear Dyn 14(11):1–8
17. Wang L, Melnik RVN (2012) Nonlinear dynamics of shape memory alloy oscillators in tuning structural vibration frequencies. Mechatronics 22:1085–1096
18. Rajagopal K, Karthikeyan A, Duraisamy P, Weldegiorgis R (2018) Bifurcation and chaos in integer and fractional order two-degree-of-freedom shape memory alloy oscillators. Complexity 1:9
19. Lagoudas DC, Machado LG, Lagoudas M (2005) Nonlinear vibration of a one-degree of freedom shape memory alloy oscillator: a numerical-experimental investigation. In: 46th AIAA/ASME/ASCE/AHS/ASC structures, structural dynamics and materials conference, Austin
20. Qidwai MA, Lagoudas DC (2000) Numerical implementation of a shape memory alloy thermomechanical constitutive model using return mapping algorithms. Int J Numer Methods Eng 47(6):1123–1168
21. Sitnikova E, Pavlovskaia E, Ing J, Wiercigroch M (2012) Experimental bifurcations of an impact oscillator with SMA constraint. Int J Bifurc Chaos 22(5):19
22. Enemark S, Savi MA, Santos IF (2015) Experimental analyses of dynamical systems involving shape memory alloys. Smart Struct Syst 15(6):1521–1542
23. Enemark S, Savi MA, Santos IF (2014) Nonlinear dynamics of a pseudoelastic shape memory alloy system—theory and experiment. Smart Mater Struct 23(8):17
24. Santos B, Savi MA (2009) Nonlinear dynamics of a nonsmooth shape memory alloy oscillator. Chaos Solitons Fractals 40(1):197–209
25. Silva LC, Savi MA, Paiva A (2013) Nonlinear dynamics of a rotordynamic nonsmooth shape memory alloy system. J Sound Vib 332:608–621
26. Rusinek R, Warminski J, Szymanski M, Kecika K, Kozik K (2017) Dynamics of the middle ear ossicles with an SMA prosthesis. Int J Mech Sci 127:163–175
27. Costa DDA, Savi MA (2017) Nonlinear dynamics of an SMA-pendulum system. Nonlinear Dyn 87:1617–1627
28. Rodrigues GV, Paiva A, Fonseca LM (2015) Nonlinear investigation of chaos and hyperchaos in a 2-DOF shape memory oscillator. In: 23rd ABCM international congress of mechanical engineering, Rio de Janeiro
29. Fonseca LM, Rodrigues GV, Savi MA, Paiva A (2019) Nonlinear dynamics of an origami wheel with shape memory alloy actuators. Chaos Solitons Fractals 122:245–261
30. Savi MA, Pacheco PMCL, Braga AMB (2002) Chaos in a shape memory two-bar truss. Int J Nonlinear Mech 37(8):1387–1395
31. Savi MA, Nogueira JB (2010) Nonlinear dynamics and chaos in a pseudoelastic two-bar truss. Smart Mater Struct 19(11):1–11
32. Bessa WM, de Paula AS, Savi MA (2013) Adaptive fuzzy sliding mode control of smart structures. Eur Phys J Spec Top 222(7):1541–1551
33. Costa DDA, Savi MA, de Paula AS, Bernardini D (2019) Chaos control of a shape memory alloy structure using thermal constrained actuation. Int J Nonlinear Mech 111:106–118
34. de Paula AS, Savi MA, Lagoudas DC (2012) Nonlinear dynamics of a SMA large-scale space structure. J Braz Soc Mech Sci Eng 34:401–412
35. Asgarian B, Salari N, Saadati B (2016) Application of intelligent passive devices based on shape memory alloys in seismic control of structures. Structures 5:161–169
36. Vignoli LL, Savi MA, El-Borgi S (2020) Nonlinear dynamics of earthquake-resistant structures using shape memory alloy composites. J Intell Mater Syst Struct 31(5):771–787
37. Gottwald GA, Melbourne I (2004) A new test for chaos in deterministic systems. Proc R Soc Lond A 460:603–611
38. Gottward GA, Melbourne I (2009) On the implementation of the 0–1 test for chaos. SIAM J Appl Dyn Syst 8:129–145
39. Bernardini D, Litak G (2016) An overview of 0–1 test for chaos. J Braz Soc Mech Sci Eng 38:1433–1450
40. Litak G, Syta A, Wiercigroch M (2009) Identification of chaos in a cutting process by the 0–1 test. Chaos Solitons Fractals 40(5):2095–2101
41. Bernardini D, Rega G, Litak G, Syta A (2013) Identification of regular and chaotic isothermal trajectories of a shape memory oscillator using the 0–1 test. Proc Inst Mech Eng Part K J Multibody Dyn 227(1):17–22
42. Savi MA, Pinto FHP, Viola F, de Paula A, Bernardini D, Litak G, Rega G (2017) Using 0–1 test to diagnose chaos on shape memory alloy dynamical systems. Chaos Solitons Fractals 103:307–324
43. Kantz H (1994) A robust method to estimate the maximal Lyapunov exponent of a time series. Phys Lett A 185(1):77–87
44. Zeng X, Eykholt R, Pielke RA (1991) Estimating the Lyapunov-exponent spectrum from short time series of low precision. Phys Rev Lett 66(25):3229
45. Rosenstein MT, Collins JJ, De Luca CJ (1993) A practical method for calculating largest Lyapunov exponents from small data sets. Physica D 65(1–2):117–134
46. Wolf A, Swift JB, Swinney HL, Vastano A (1985) Determining Lyapunov exponents from a time series. North-Holland Phys Publ Div 16:285–317
47. Stefanski A, Kapitaniak T (2003) Estimation of the dominant Lyapunov exponent of non-smooth systems on the basis of maps synchronization. Chaos Solitions Fractals 15(2):233–244
48. Dabrowski A (2012) Estimation of the largest Lyapunov exponent from perturbation vector and its derivative do product. Nonlinear Dyn 67(1):283–291
49. Soriano DC, Fazanaro FI, Suyama R, Oliveira JR, Attux R, Madrid MK (2012) A method for Lyapunov spectrum estimation using cloned dynamics and its application to the discontinuously-excited FitzHugh–Nagumo model. Nonlinear Dyn 67(1):413–424
50. Machado LG, Lagoudas DC, Savi MA (2009) Lyapunov exponents estimation for hysteretic systems. Int J Solids Struct 46(6):1269–1286
51. Syta A, Bernardini D, Litak G, Savi MA, Jonak K (2020) A comparison of different approaches to detect the transitions from regular to chaotic motions in SMA oscillator. Meccanica 55:1295–1308
52. Eckmann JP, Oliffson-Kamphorst S, Ruelle D (1987) Recurrence plots of dynamical systems. Europhys Lett 4:973–977
53. Falk F (1980) Model free-energy, mechanics and thermodynamics of shape memory alloys. ACTA Metal 28:1773–1780

**Publisher's Note** Springer Nature remains neutral with regard to jurisdictional claims in published maps and institutional affiliations.